

See discussions, stats, and author profiles for this publication at: <https://www.researchgate.net/publication/263959894>

Influence of Gold Nanoparticles Anchored to Carbon Nanotubes on Formation and Decomposition of Li₂O₂ in Nonaqueous Li-O₂ Batteries

ARTICLE *in* THE JOURNAL OF PHYSICAL CHEMISTRY C · APRIL 2014

Impact Factor: 4.77 · DOI: 10.1021/jp500597m

CITATIONS

6

READS

10

4 AUTHORS, INCLUDING:



Xiangxin Guo

Chinese Academy of Sciences

62 PUBLICATIONS 593 CITATIONS

SEE PROFILE

Influence of Gold Nanoparticles Anchored to Carbon Nanotubes on Formation and Decomposition of Li_2O_2 in Nonaqueous Li– O_2 Batteries

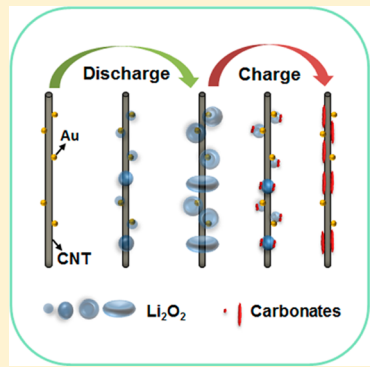
Wugang Fan,[†] Xiangxin Guo,^{*,†} Dongdong Xiao,[‡] and Lin Gu[‡]

[†]State Key Laboratory of High Performance Ceramics and Superfine Microstructure, Shanghai Institute of Ceramics, Chinese Academy of Sciences, 1295 Dingxi Road, Shanghai 200050, China

[‡]Beijing National Laboratory for Condensed Matter Physics, Institute of Physics, Chinese Academy of Sciences, Beijing 100190, China

S Supporting Information

ABSTRACT: Gold nanoparticles (AuNPs) anchored to vertically aligned carbon nanotubes (VACNTs) act as additional nucleation sites for the Li_2O_2 growth, leading to the decreased size while increased density of Li_2O_2 particles in process of discharge. Correspondingly, at the deep discharge to 2.0 V the batteries show increased specific capacity. Upon charge, the AuNPs exhibit promotion effect on the Li_2O_2 decomposition by improving the conduction property of the discharge-formed particles, rather than by imposing the conventional electrocatalytic effect on the oxygen evolution reaction. Moreover, the AuNPs show promotion effect on decomposition of carbonate species arising from the side reactions. These effects consequently lead to the reduced charge overpotentials and extended cycle operation of the batteries. The results here provide a new as well as clear picture on the role of incorporated AuNPs in the Li_2O_2 formation and decomposition, which would be helpful for better understanding and constructing of high-performance air cathodes.



INTRODUCTION

The interest in rechargeable nonaqueous Li–air or Li– O_2 batteries surges in recent years because they can deliver exceptionally higher specific energy than state-of-the-art Li-ion batteries.^{1–6} The Li– O_2 batteries produce large values of discharge capacity by forming a large amount of crystalline Li_2O_2 particles and regain the storage ability by decomposing them upon charging. It is well acknowledged that the current Li– O_2 batteries face critical problems including the large polarization, limited cycle life, and poor rate capability.^{7–16} These problems are closely related to the kinetics of Li_2O_2 growth and decomposition in the repeated discharge and charge processes. In addition, owing to instability of electrolytes and cathodes, the carbonate species as the main component of side products should also be concerned because of their deleterious influence on the reversibility of Li_2O_2 formation and decomposition. It is clear that comprehensive elucidation of growth as well as decomposition mechanism of Li_2O_2 during battery operation is crucial if solutions to overcome the aforementioned problems are to be found. In our previous work, the morphology and chemical composition of Li_2O_2 changing with cycles were studied by using the cathodes of vertically aligned carbon nanotubes (VACNTs) directly grown on the stainless-steel networks.¹⁷ The processes with respect to the growth of abacus-ball-shaped Li_2O_2 particles as well as rust-like carbonates were described. Very recently, aimed to decrease the large polarization and improve the rate perform-

ance, many researches were reported on incorporation of noble-metal nanoparticles into the carbon-based cathodes.^{18–21} Nevertheless, the influence of these nanoparticles on both formation and decomposition of Li_2O_2 in comparison to that of pure carbon-based cathodes has been scarcely studied.

In addition, incorporation of Au nanoparticles (AuNPs) or their derivatives into the carbon-based cathodes in the nonaqueous Li– O_2 batteries has attracted much attention.^{22–26}

Some researchers found that the AuNPs exhibited good oxygen reduction reaction (ORR) or/and oxygen evolution reaction (OER) activities.^{22–24} More encouragingly, the batteries with the nanoporous gold (NPG) cathodes and the electrolytes based on dimethyl sulfoxide (DMSO) performed a > 99% purity of Li_2O_2 formation during discharge and complete Li_2O_2 decomposition upon charge for as long as 100 cycles, highly implying that the AuNPs could be one of sustainable materials for constructing highly efficient cathodes.²⁵ In contrast, McCloskey et al.²⁶ found no catalytic activity of Au nanoparticles compared to the pure carbon in OER when the Li_2O_2 was the dominant discharge product. They suggested that the inclusion of AuNPs might affect transport issues such as the relevant discharge electrodeposit's conductivity or binding energy for full O_2 evolution during charging after deep

Received: January 18, 2014

Revised: March 20, 2014

Published: March 21, 2014



discharge. Furthermore, in their subsequent publication,²⁷ they even pointed out that the nanoporous Au cathodes might not be stable against the DMSO-based electrolytes. In addition to the above discussions, some recent papers disclosed that the surface sites on carbon surfaces or the added nanoparticles could modify the morphology, defect chemistry, or crystallinity of Li₂O₂ formed upon discharge, which led to reduced charge overpotentials.^{20,28,29} Whether such influence is also imposed by AuNPs has not ever been reported. Briefly speaking, previous reports imply that the utilization of Au could promote the Li₂O₂ decomposition through conventional catalytic effect or improvement of transport property. Which factor plays the important role is not clear. As a result, here, the AuNPs anchored to vertical-aligned carbon nanotubes (AuNPs/VACNTs) were synthesized, and their influence on Li₂O₂ formation and decomposition in comparison to the pure VACNTs was investigated. Because of the direct growth of VACNTs on stainless-steel networks, both VACNTs and AuNPs/VACNTs can be used as free-standing cathodes without incorporating binders or other conductive additives. Such configuration allows for easily detecting the change in morphology and chemical composition of reaction products with cycles. It is found that the incorporated AuNPs provide additional nucleation sites for the Li₂O₂ growth during discharge, leading to the increased specific capacity. Meanwhile, the Li₂O₂ particles formed on the AuNPs/VACNTs have smaller size than those on the pure VACNTs. This leads to improved transport property of the discharge products, thus reducing the following charge potentials. Moreover, it is also found that the AuNPs help decompose the carbonates arising from the electrolyte decomposition. Consequently, the incorporation of AuNPs leads to the reduced charge potentials and extended cycle operation of the ether-based Li—O₂ batteries.

■ EXPERIMENTAL SECTION

The synthesis of AuNPs was carried out by reduction of HAuCl₄ in distilled water. Typically, a volume of 50 mL of aqueous solution containing 0.3 mM sodium citrate (C₆H₅Na₃O₇·2H₂O, Sinopharm Chemical Reagent Co., Ltd.) and 0.2 mM HAuCl₄ (Aladdin Chemical Co., Ltd.) was prepared by adding the two reagents into distilled water at 4 °C. Subsequently, 1 mL of 0.1 M NaBH₄ solution at 4 °C was added dropwise into the above solution under vigorous stirring. The color of the solution turned to reddish purple immediately, indicating formation of AuNPs. The resulting red solution was aged for 2 h to ensure that the reduction reaction was completed.

The vertically aligned carbon nanotubes grown on the stainless steel meshes were purchased from Microphase Co., Ltd., in Japan, which were prepared by the chemical vapor deposition. They were immersed into the as-prepared AuNPs solution in glass pots. The solutions were mildly stirred for 90 min in a dark place at room temperature to load the AuNPs into the carbon nanotube arrays. Then they were rinsed with distilled water and ethanol, respectively. After drying at 80 °C for 2 h in an oven, the AuNPs/VACNTs electrodes were annealed at 450 °C for 30 min in air to remove the impurities on the surface of gold. The annealed AuNPs/VACNTs were kept at 80 °C in vacuum for overnight before use. The Au content in the AuNPs/VACNTs was measured by electron probe microanalysis (JXA-8100, JEOL). The mass of the carbon nanotubes was approximately 2.0 mg cm⁻², and the

specific surface area was around 80 m² g⁻¹ measured by the ASAP 2010 system.

Each battery in Swagelok-type was assembled in an Ar-filled glovebox with oxygen and moisture levels below 0.1 ppm, consisting of a lithium foil, a VACNTs or AuNPs/VACNTs cathode, and a glass fiber (Whatman) separator soaked with the electrolyte. The detailed assembly and battery testing procedures for Li—O₂ cells with the 1.0 M LiTFSI:DME can refer to our previous reports.¹⁷ The specific capacity was calculated based on the mass of carbon nanotubes for VACNTs and AuNPs plus VACNTs for the AuNPs/VACNTs cathode, respectively.

For the Li—O₂ batteries with the DME-based electrolyte, the cells were purged for 10 min with high-purity O₂ in a dry Ar/O₂-filled box and then sealed and rested for 2 h before testing. The detailed process can be found in our previous report.¹⁷ The discharge and charge measurements were conducted on an Arbin BT 2000 cycler.

Raman spectroscopy was recorded on Thermo DXR with an excitation wavelength of 532 nm. The cathodes tested with the DME-based electrolytes were rinsed with the DME solvent in the Ar-filled glovebox before drying on a filter paper. XRD measurement of the cathodes disassembled from the tested cells was conducted using a diffractometer (D8 Discover, Bruker) with Cu K α radiation in a reflection mode. The samples were sealed into a stainless steel sample holder with a Be window. Scanning electron microscopy (SEM) images were recorded by a FEI Magellan 400. High-resolution transmission electron microscopy (HRTEM) characterization was conducted by JEOL JSM-6700F and JEM-ARM200F microscope with spherical aberration (C_s) corrector. X-ray photoelectron spectra (XPS) were carried out by ESCAlab-250 with an Al anode source. The samples were presputtered at a pressure of 3 × 10⁻⁹ Pa. All the samples during transferring were protected by an Ar atmosphere. The electrochemical impedance spectroscopy (EIS) was measured with an electrochemical workstation (Autolab) in frequency range of 0.1–10⁵ Hz under an ac voltage amplitude of 20 mV. The cyclic voltammetry (CV) and linear sweep voltammetry (LSV) measurements were conducted with a glassy carbon as working electrode. VACNTs and AuNPs/VACNTs dispersed in ethanol were coated on the surface of glassy carbon with Nafion as binder. Platinum meshes (~1 cm²) and Ag/Ag⁺ electrodes were used as the counter electrodes and reference electrodes, respectively. For analysis of the lithium carbonate decomposition, Li₂CO₃ powders (metal trace 99.99%, J&K Scientific Ltd.) were dissolved into distilled water by stirring, which were added dropwise onto nanoporous Au and porous carbon (carbon paper, TGP-H-060, Toray). The nanoporous Au was prepared by dealloying of Au/Ag leaf (Nanjing Jinling Goldfoil Co., Ltd.) according to ref 30.

■ RESULTS AND DISCUSSION

Characterization of AuNPs/VACNTs Cathodes. Figure 1a shows the surface morphology of a typical cathode detected by SEM. It can be seen that many tiny particles distributing on the VACNTs. Energy dispersive spectrum (EDS) analysis reveals that these tiny particles are attributed to Au, as shown in Figure 1b. Note that the AuNPs preferentially adhere to the carbon nanotubes which locate at the periphery of the VACNTs forests. The amount of AuNPs in the central part is probably less than that in the outside part. The mass percentage of AuNPs in the cathode is 3.0–5.0 wt %. TEM

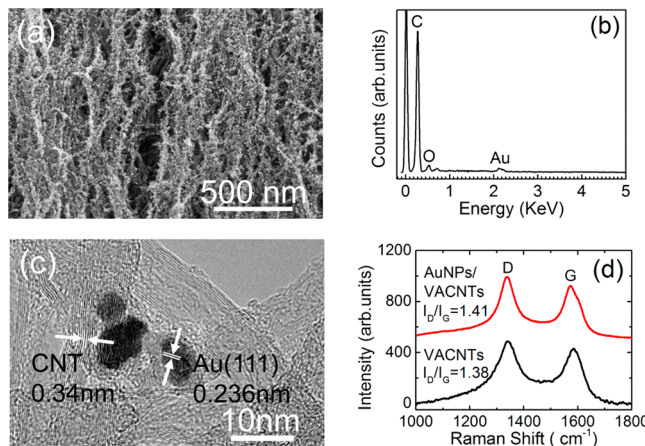


Figure 1. (a) Typical SEM image of AuNPs/VACNTs. (b) EDS spectrum of AuNPs/VACNTs. (c) Typical TEM image of AuNPs/VACNT. (d) Raman spectra of the pristine VACNTs in comparison with that of the AuNPs/VACNTs.

observation reveals that the AuNPs are in size of approximately 5–10 nm, as indicated in Figure 1c. The lattice fringes for the crystalline Au and the shells of carbon nanotubes can be clearly identified. To examine if the defect density of VACNTs changes after the incorporation of AuNPs, Raman spectroscopy measurements were carried out on both VACNTs and AuNPs/VACNTs. The results given in Figure 1d show that the defect density of nanotubes for the two-type cathodes has no detectable difference, as indicated by the similar peak intensity ratio of D-band versus G-band.

Influence of the Incorporated AuNPs on the Li₂O₂ Formation during Discharge. The first discharge and charge behaviors of the batteries with the pure VACNTs and AuNPs/VACNTs cathodes are investigated. The typical curves measured in potential range of 2–4.5 V at the current density of 0.1 mA cm⁻² are shown in Figure 2a. From the figure, it is

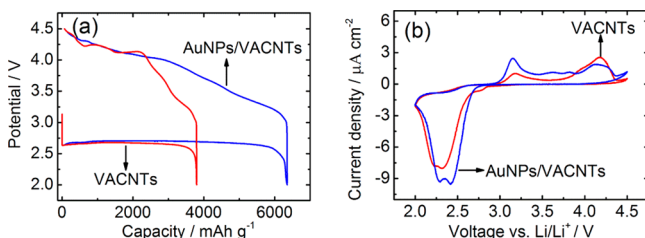


Figure 2. (a) First cycle curves for the Li/DME-LiTFSI/O₂ cells with the pristine VACNTs and AuNPs/VACNTs cathodes, measured at the current density of 0.1 mA cm⁻². (b) Cyclic voltammetry curves of the pristine VACNTs and AuNPs/VACNTs cathodes in TEGDME-based electrolyte under Ar:O₂ (80:20 vol %) atmosphere between 2 and 4.5 V vs Li/Li⁺. The scan rate is 20 mV s⁻¹.

obvious that the discharge capacity of 6350 mAh g⁻¹ with respect to the AuNPs/VACNTs is much larger than that of 3800 mAh g⁻¹ corresponding to the pure VACNTs. The cyclic voltammetry (CV) measurement also indicates that the AuNPs/VACNTs show a higher cathodic current than the sole VACNTs (Figure 2b). Note that the two ORR peaks in CV can be attributed to the LiO₂ and Li₂O₂ formation, according to the previous report which indicates that the ORR proceeds through the reactions (1) O₂ + Li⁺ + e⁻ → LiO₂ and (2) 2LiO₂ → Li₂O₂ + O₂.³¹ These results clearly indicate that

the incorporation of AuNPs promotes the ORR reactions and increases the discharge capacity. In addition, a slight increase of discharge potential by the incorporation of AuNPs can be seen in Figure 2a.

In order to visualize the influence of AuNPs on the Li₂O₂ formation, the morphological changes of cathode with depth of discharge for the VACNTs and Au/VACNTs cathodes are comparatively investigated. As shown in Figures 3a and 3b, at

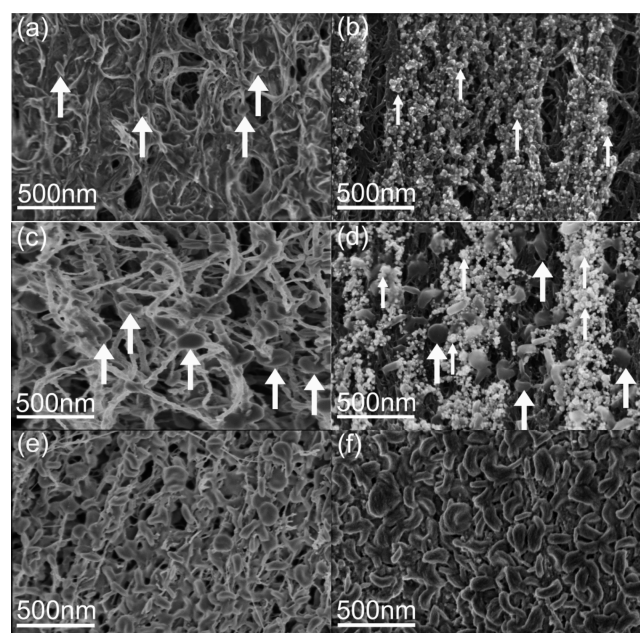


Figure 3. SEM images for the VACNTs and AuNPs/VACNTs cathodes after different discharge processes: (a) VACNTs and (b) AuNPs/VACNTs cathodes discharged to a capacity of ~500 mAh g⁻¹; (c) VACNTs and (d) AuNPs/VACNTs discharged to a capacity of ~1200 mAh g⁻¹; (e) VACNTs and (f) AuNPs/VACNTs discharged to 2.0 V with capacities of 3800 and 6350 mAh g⁻¹, respectively. The small arrows point to the Li₂O₂ particles deposited on the AuNPs and the large ones to those grown around the VACNTs.

the discharge capacity of 500 mAh g⁻¹, while some Li₂O₂ particles in size of 50–70 nm grown around the nanotubes can be found for the VACNTs cathode, many particles smaller than 30 nm are grown around the Au nanoparticles in the case of the AuNPs/VACNTs. Note that the formation of crystalline Li₂O₂ particles has been confirmed by XRD measurement as shown in Figure S1. As the discharge capacity increases to 1200 mAh g⁻¹, the Li₂O₂ particles become larger with the nearly uniform size of ~120 nm for the VACNTs cathode as shown in Figure 3c. For the AuNPs/VACNTs, two kinds of particles in different size can be seen in Figure 3d. One type of particles in size of ~120 nm, which are very similar to those as observed in Figure 3c, indicating that they most probably grow around the nanotubes where the AuNPs are absent. The other type of particles in size of ~40 nm are most probably attributed to the enlarged Li₂O₂ crystals grown around the AuNPs. As the batteries are discharged to 2.0 V, as shown in Figures 3e and 3f, both surfaces of the two types of cathodes are covered by the toroidal Li₂O₂ particles which have the nearly similar size of 160 nm on average. The numerical density of particles for the AuNPs/VACNTs is larger than that for the VACNTs, in agreement with the fact that the incorporation of AuNPs increases the discharge capacity.

Complementary to the above SEM measurement, the TEM technique was applied to study morphological change of the Li_2O_2 particles with depth of discharge for the AuNPs/VACNTs cathodes. Figure 4a shows the morphology of AuNPs

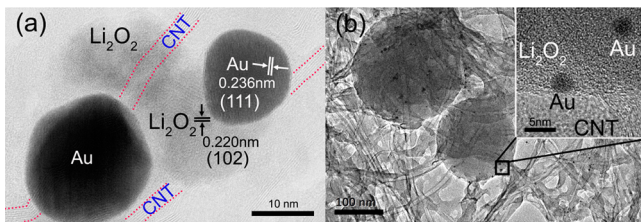


Figure 4. TEM images for (a) the AuNPs/VACNTs cathode with a discharge capacity of 500 mAh g^{-1} and (b) the AuNPs/VACNTs cathode discharged to 2 V or with a discharge capacity of 6350 mAh g^{-1} .

after the discharge to 500 mAh g^{-1} . The interface between the crystalline Li_2O_2 and the AuNPs can be clearly observed, which indicates that the AuNPs behave as additional nucleation sites for the Li_2O_2 growth. After the discharge to 2.0 V , the large Li_2O_2 particles in size of $\sim 160 \text{ nm}$ can be seen in Figure 4b. Interestingly, both the VACNTs and the AuNPs are surrounded by these large Li_2O_2 particles, indicating that the small particles initiated by both of them eventually emerge to large ones. Such a picture for the Li_2O_2 growth in the presence of both carbon electrodes and nanoparticle additives is reported for the first time according to our knowledge.

Early Decomposition of the Li_2O_2 Particles during Charge with the Incorporated AuNPs. According to Figure 2a, it can be calculated that the ratio of the charge capacity below 4.0 V to the discharge capacity is approximately 65% in the case of AuNPs/VACNTs cathode, while it is only 35% for the VACNTs. This is consistent with the fact that the former shows the larger intensity of the anodic peak corresponding to the OER process at approximately 3.2 V than the latter (Figure 2b). These results imply that more Li_2O_2 are decomposed in the presence of AuNPs. To exaggerate such an effect of AuNPs on the Li_2O_2 decomposition, the batteries with both types of cathodes were discharged to the same capacity of 3000 mAh g^{-1} and subsequently recharged to 3.75 V . Then the operated batteries were disassembled and cathodes detected by SEM. As shown in Figure 5, while for the VACNTs cathode many abacus-ball-shaped Li_2O_2 particles in size of $40\text{--}50 \text{ nm}$ are still visible (Figure 5a), fewer Li_2O_2 particles are observable for the AuNPs/VACNTs cathode (Figure 5b), clearly indicating early decomposition of the Li_2O_2 in the presence of AuNPs.

Two causes are possibly responsible for the above difference. One is the inclusion of AuNPs can improve the conduction

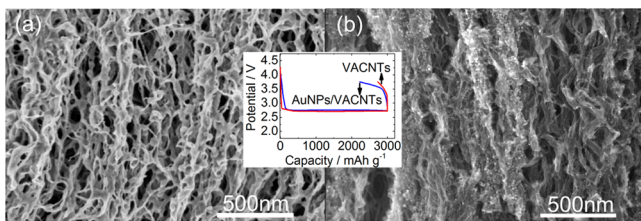


Figure 5. SEM images and discharge-charge profiles for (a) the pristine VACNT cathode and (b) the AuNPs/VACNTs one charged to 3.75 V following discharged to a capacity of 3000 mAh g^{-1} .

properties of the formed Li_2O_2 particles. This is especially true under conditions of limited depth of discharge, concerning the reduced size of Li_2O_2 particles as shown in Figure 3d. Consistently, impedance spectroscopy measurement in Figure 6a indeed reveals a smaller resistance for the AuNPs/VACNTs

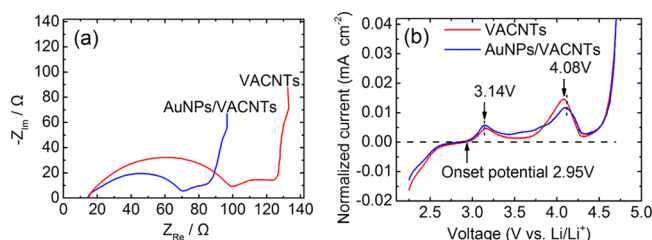


Figure 6. (a) Electrochemical impedance spectroscopy of the $\text{Li}-\text{O}_2$ cells with VACNTs and AuNPs/VACNTs cathodes discharged to 3000 mAh g^{-1} . (b) Linear sweep voltammetry for VACNTs and AuNPs/VACNTs after a hold at 2.25 V for 1 h . 2.95 V represents the onset potential for charge process, and peaks at 3.14 and 4.08 V are corresponding to the decomposition of Li_2O_2 and carbonate species, respectively.

than for the VACNTs after the discharge to 3000 mAh g^{-1} . As a result, the particles grown around the AuNPs with the reduced size can lead to an earlier Li_2O_2 decomposition upon charge for the AuNPs/VACNTs than for the VACNTs. The other is the catalytic effect of AuNPs on the Li_2O_2 decomposition. To examine if this effect exists, measurement of the linear sweep voltammetry (LSV) was carried out on the VACNTs and the AuNPs/VACNTs in the TEGDME: LiClO_4 solution. The glassy carbon electrodes coated with the testing materials were used as the working electrodes. Each measurement was conducted by first holding the voltage at 2.25 V for 1 h to deposit Li_2O_2 on the working electrode and then sweeping the voltage from 2.25 to 4.7 V (vs Li/Li^+) at a scan rate of 0.1 mV s^{-1} . When the potential being scanned from 2.25 to 4.7 V , the onset potential of oxygen evolution for the AuNPs/VACNTs is nearly the same as that for the VACNTs (i.e., both are at $\sim 2.95 \text{ V}$), as shown in Figure 6b. According to ref 32, the above result indicates that the AuNPs/VACNTs cathode has no better catalytic effect on the OER compared to the VACNTs. This result is consistent with that in the previous report, which also revealed that the AuNPs do not show better catalytic effect compared to the pure carbon.²⁶ Therefore, it can be concluded that the early decomposition of Li_2O_2 in the AuNPs/VACNTs cathodes upon charge is attributed to the more conductive Li_2O_2 particles induced by the incorporated AuNPs, rather than their electrocatalytic effect.

Reduction of Li_2CO_3 Accumulation during Cycles with the Incorporated AuNPs. XPS analysis was carried out for the cathodes of AuNPs/VACNTs and pure VACNTs after cycling with cutoff capacity of 1100 mAh g^{-1} . The peak intensity corresponding to the Li carbonate for the former after the 16th discharge is found to be weaker than for the latter after the 8th discharge, as shown in Figure 7a. This clearly indicates that the Au incorporated into the VACNTs can promote the decomposition of carbonate from side reactions during cycle operation. To further confirm this point, both the composites of porous Au and Li_2CO_3 particles and those of porous carbon paper and Li_2CO_3 particles were prepared. The charge behaviors of these composite electrodes were investigated in the cells with the Li anodes and the DME-based electrolytes. As can be seen in Figure 7b, there is a broad platform at

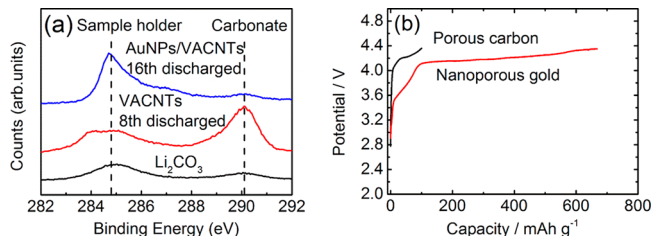


Figure 7. (a) C1s XPS spectra for the VACNTs cathode after the 8th discharge and the AuNPs/VACNTs cathode after the 16th discharge. (b) Charge curves for the electrodes composed of Li_2CO_3 and nanoporous (NP) Au and those composed of Li_2CO_3 and porous carbon.

approximately 4.2 V for Au/ Li_2CO_3 composites. According to ref 33, this platform can be attributed to Li_2CO_3 decomposition. In contrast, the porous carbon/ Li_2CO_3 composites do not show such broad platform during charge (Figure 7b). After charging, XRD measurement reveals disappearance of Li_2CO_3 peaks in the porous Au/ Li_2CO_3 electrode (Figure S2). This clearly indicates that the AuNPs have the promotion effect on the Li_2CO_3 decomposition.

Previous analysis indeed indicates that the nanoporous Au can decompose the added Li_2CO_3 . Note that occurrence of such decomposition process means that the AuNPs surface should be preferentially exposed to the liquid electrolyte at the initial stage of charge during battery operation because most of the carbonate species result from the interaction between the Li_2O_2 and the electrolyte. This point is truly indicated by the TEM characterization as shown in Figures 8a and 8b. When the

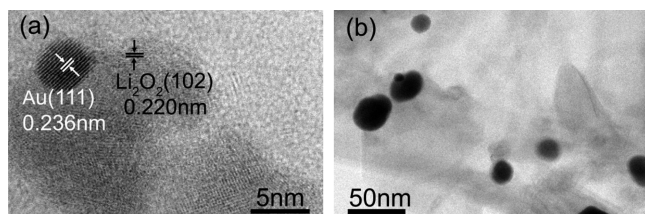


Figure 8. TEM images for the AuNPs/VACNTs cathode being charged to 3.75 V following discharged to a capacity of 3000 mAh g^{-1} at (a) high and (b) low magnification.

battery is charged to 3.75 V following the discharge to a capacity of 3000 mAh g^{-1} , the surface of AuNPs at least partially exposes. This also implies that the AuNPs are preferential sites for the Li_2O_2 decomposition in comparison to the VACNTs. As a result, during charge the AuNPs first accelerates decomposition of Li_2O_2 and then helps remove the carbonate species induced by the side reactions.

Consequently, the batteries with the AuNPs/VACNTs cathodes exhibit the smaller charge potentials and larger cycle number than those with the sole VACNTs cathode, as shown in Figures 9a and 9b. The charge overpotential of the first and eighth cycle is smaller for the former than for the latter. Consistently, the batteries with the AuNPs/VACNTs cathodes can run for 16 cycles with retaining the initial capacity, while those with the VACNTs can only run for 8 cycles (Figure S3). Before we draw the conclusions, two points are worthwhile mentioning here. One is the concern of Au oxidation as the charge potential is over 4.0 V.^{25,27} By careful examination of the discharge/charge, CV (Figures 2a and 2b) and linear sweep voltammetry curves (Figure 6b), it can be found that though

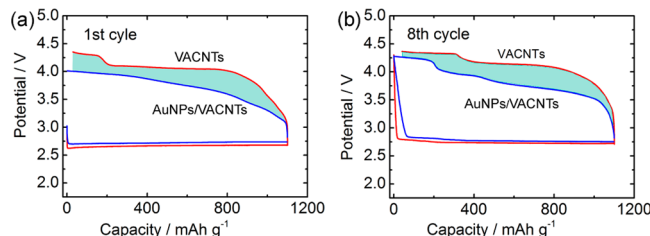


Figure 9. For the batteries with LiTFSI:DME electrolytes, (a) 1st and (b) 8th discharge–charge profiles with the discharge cutoff capacity of 1100 mAh g^{-1} in the voltage range of 2–4.35 V of VACNTs and AuNPs/VACNTs at 0.1 mA cm^{-2} .

the oxidation of AuNPs cannot be completely excluded, the reaction arising from the Au oxidation is much weaker than that from the decomposition of carbon-based cathodes or electrolytes. This is most probably attributed to the small amount of AuNPs incorporated in the VACNTs or the passivation of AuNPs surface by coating of the reaction products. Therefore, the charge cutoff of 4.35 V used here should not affect the main conclusions. The other one is the concern of decomposition of DME in the $\text{Li}-\text{O}_2$ battery. Note that the purpose of this article is to clarify the influence of incorporated AuNPs on formation and decomposition of reaction products including Li_2O_2 and carbonate species. This requirement can be well met by DME, which is relatively stable to produce Li_2O_2 during discharge and unstable to produce carbonate-based side products upon charge. In addition, the DME solvent is easy to remove from the discharged or charged cathode materials, which facilitates investigation of morphology and crystallinity changes of the cathode materials.

CONCLUSIONS

The free-standing cathodes composed of AuNPs anchored to VACNTs have been synthesized. Their role in the Li_2O_2 formation and decomposition is studied. In comparison to the VACNTs, the AuNPs behave as the additional nucleation sites for the Li_2O_2 growth, forming the Li_2O_2 particles with the increased density as well as the reduced size in process of discharge. After the deep discharge to 2.0 V, the large particles surrounding both VACNTs and AuNPs are formed. The reduced size and the configuration of AuNPs embedded in the Li_2O_2 particles improve the conduction property of the discharge products, which takes responsibility for the early Li_2O_2 decomposition upon charge. Meanwhile, the AuNPs have the promotion effect on decomposition of carbonate species arising from the electrolyte decomposition on charge. Consequently, the incorporation of AuNPs leads to the reduced charge potentials and extended cycle number during operation of the $\text{Li}-\text{O}_2$ batteries with the DME-based electrolytes. The disclosed mechanism here would be helpful for better understanding of the influence of noble-metal catalysts on the reaction kinetics in the nonaqueous $\text{Li}-\text{O}_2$ batteries.

ASSOCIATED CONTENT

Supporting Information

Figure S1: XRD patterns of the AuNPs/VACNTs cathodes after first discharge and charge; Figure S2: XRD measurement for the NP-Au electrode on stainless steel mesh, the NP-Au composited with Li_2CO_3 one, and the charged NP-Au composited with Li_2CO_3 one; Figure S3: the capacity and

discharge potential as a function of cycle number and the corresponding Coulombic efficiency at 0.1 mA cm^{-2} . This material is available free of charge via the Internet at <http://pubs.acs.org>.

AUTHOR INFORMATION

Corresponding Author

*Tel 0086-21-52411032, Fax 0086-21-52411802, e-mail XXGuo@mail.sic.ac.cn (X.G.).

Notes

The authors declare no competing financial interest.

ACKNOWLEDGMENTS

This work was supported by the Key Project of the Chinese Academy of Sciences under Grant No. KGZD-EW-202-2, Sony Corporation, and the Science Foundation for Young Researchers of State Key Laboratory of High Performance Ceramics and Superfine Microstructures (SKL201104), National Natural Science Foundation of China (No.11174334). Dr. Keisuke Shimizu, Dr. Hiroyuki Morioka, Dr. Hisashi Kajiura, and Dr. Yongming Li are acknowledged for helpful discussions.

REFERENCES

- (1) Abraham, K. M.; Jiang, Z. A Polymer Electrolyte-Based Rechargeable Lithium/Oxygen Battery. *J. Electrochem. Soc.* **1996**, *143*, 1–5.
- (2) Girishkumar, G.; McCloskey, B.; Luntz, A. C.; Swanson, S.; Wilcke, W. Lithium-Air Battery: Promise and Challenges. *J. Phys. Chem. Lett.* **2010**, *1*, 2193–2203.
- (3) Nanda, J.; Bilheux, H.; Voisin, S.; Veith, G. M.; Archibald, R.; Walker, L.; Allu, S.; Dudney, N. J.; Pannala, S. Anomalous Discharge Product Distribution in Lithium-Air Cathodes. *J. Phys. Chem. C* **2012**, *116*, 8401–8408.
- (4) Bruce, P. G.; Freunberger, S. A.; Hardwick, L. J.; Tarascon, J. M. Li-O₂ and Li-S Batteries with High Energy Storage. *Nat. Mater.* **2012**, *11*, 19–29.
- (5) Xia, C.; Waletzko, M.; Peppler, K.; Janek, J. Silica Nanoparticles as Structural Promoters for Oxygen Cathodes of Lithium–Oxygen Batteries. *J. Phys. Chem. C* **2013**, *117*, 19897–19904.
- (6) Guo, X. X.; Huang, S. T.; Zhao, N.; Cui, Z. H.; Fan, W. G.; Li, C. L.; Li, H. Rapid Development and Critical Issues of Secondary Lithium-Air Batteries. *J. Inorg. Mater.* **2014**, *28*, 113–123.
- (7) Mitchell, R. R.; Gallant, B. M.; Thompson, C. V.; Shao-Horn, Y. All-Carbon-Nanofiber Electrodes for High-Energy Rechargeable Li-O₂ Batteries. *Energy Environ. Sci.* **2011**, *4*, 2952–2958.
- (8) Oh, H. S.; Nazar, L. F. Oxide Catalysts for Rechargeable High-Capacity Li–O₂ Batteries. *Adv. Energy Mater.* **2012**, *2*, 903–910.
- (9) Nasibulin, E.; Xu, W.; Engelhard, M. H.; Nie, Z.; Burton, S. D.; Cosimescu, L.; Gross, M. E.; Zhang, J.-G. Effects of Electrolyte Salts on the Performance of Li–O₂ Batteries. *J. Phys. Chem. C* **2013**, *117*, 2635–2645.
- (10) Laoire, C. Ó.; Mukerjee, S.; Plichta, E. J.; Hendrickson, M. A.; Abraham, K. M. Rechargeable Lithium/TEGDME-LiPF₆/O₂ Battery. *J. Electrochem. Soc.* **2011**, *158*, A302–A308.
- (11) Lim, H.-D.; Park, K.-Y.; Song, H.; Jang, E. Y.; Gwon, H.; Kim, J.; Kim, Y. H.; Lima, M. D.; Robles, R. O.; Lepró, X.; et al. Enhanced Power and Rechargeability of a Li–O₂ Battery Based on a Hierarchical-Fibril CNT Electrode. *Adv. Mater.* **2013**, *25*, 1348–1352.
- (12) Li, F. J.; Ohnish, R.; Yamada, Y.; Kubota, J.; Domen, K.; Yamada, A.; Zhou, H. S. Carbon Supported TiN Nanoparticles: An Efficient Bifunctional Catalyst for Non-Aqueous Li–O₂ Batteries. *Chem. Commun.* **2013**, *49*, 1175–1177.
- (13) Shao, Y. Y.; Ding, F.; Xiao, J.; Zhang, J.; Xu, W.; Park, S.; Zhang, J.-G.; Wang, Y.; Liu, J. Making Li–Air Batteries Rechargeable: Material Challenges. *Adv. Funct. Mater.* **2013**, *23*, 987–1004.
- (14) Monaco, S.; Soavi, F.; Mastragostino, M. Role of Oxygen Mass Transport in Rechargeable Li/O₂ Batteries Operating with Ionic Liquids. *J. Phys. Chem. Lett.* **2013**, *4*, 1379–1382.
- (15) Hartmann, P.; Bender, C. L.; Vračar, M.; Dürr, A. K.; Garsuch, A.; Janek, J.; Adelhelm, P. A Rechargeable Room-Temperature Sodium Superoxide (NaO₂) Battery. *Nat. Mater.* **2013**, *12*, 228–232.
- (16) Guo, X. X.; Zhao, N. The Role of Charge Reactions in Cyclability of Lithium–Oxygen Batteries. *Adv. Energy Mater.* **2013**, *3*, 1413–1416.
- (17) Fan, W. G.; Cui, Z. H.; Guo, X. X. Tracking Formation and Decomposition of Abacus-Ball-Shaped Lithium Peroxides in Li–O₂ Cells. *J. Phys. Chem. C* **2013**, *117*, 2623–2627.
- (18) Thapa, A. K.; Shin, T. H.; Ida, S.; Sumanasekera, G. U.; Sunkara, M. K.; Ishihara, T. Gold-Palladium Nanoparticles Supported by Mesoporous β-MnO₂ Air Electrode for Rechargeable Li–Air Battery. *J. Power Sources* **2012**, *220*, 211–216.
- (19) Lu, J.; Lei, Y.; Lau, K. C.; Luo, X. Y.; Du, P.; Wen, J. G.; Assary, R. S.; Das, U.; Miller, D. J.; Elam, J. W. A Nanostructured Cathode Architecture for Low Charge Overpotential in Lithium–Oxygen Batteries. *Nat. Commun.* **2013**, *4*, 2383.
- (20) Xu, J. J.; Wang, Z. L.; Xu, D.; Zhang, L. L.; Zhang, X. B. Tailoring Deposition and Morphology of Discharge Products Towards High-Rate and Long-Life Lithium–Oxygen Batteries. *Nat. Commun.* **2013**, *4*, 2438.
- (21) Sheng, W. C.; Lee, S. W.; Crumlin, E. J.; Chen, S.; Shao-Horn, Y. Synthesis, Activity and Durability of Pt Nanoparticles Supported on Multi-walled Carbon Nanotubes for Oxygen Reduction. *J. Electrochem. Soc.* **2013**, *158*, B1398–B1404.
- (22) Lu, Y.-C.; Xu, Z. C.; Gasteiger, H. A.; Chen, S.; Hamad-Schifferli, K.; Shao-Horn, Y. Platinum–Gold Nanoparticles: A Highly Active Bifunctional Electrocatalyst for Rechargeable Lithium–Air Batteries. *J. Am. Chem. Soc.* **2010**, *132*, 12170–12171.
- (23) Kumar, S.; Selvaraj, C.; Munichandraiah, N.; Scanlonb, L. G. Gold Nanoparticles Anchored Reduced Graphene Oxide as Catalyst for Oxygen Electrode of Rechargeable Li–O₂ Cells. *RSC Adv.* **2013**, *3*, 21706–21714.
- (24) Marinaro, M.; Riek, U.; Eswara Moorthy, S. K.; Bernhard, J.; Kaiser, U.; Wohlfahrt-Mehrens, M.; Jörissen, L. Au-Coated Carbon Cathodes for Improved Oxygen Reduction and Evolution Kinetics in Aprotic Li–O₂ Batteries. *Electrochem. Commun.* **2013**, *37*, 53–56.
- (25) Peng, Z. Q.; Freunberger, S. A.; Chen, Y. H.; Bruce, P. G. A Reversible and Higher-Rate Li–O₂ Battery. *Science* **2012**, *337*, 563–566.
- (26) McCloskey, B. D.; Scheffler, R.; Speidel, A.; Bethune, D. S.; Shelby, R. M.; Luntz, A. C. On the Efficacy of Electrocatalysis in Nonaqueous Li–O₂ Batteries. *J. Am. Chem. Soc.* **2011**, *133*, 18038–18041.
- (27) McCloskey, B. D.; Valery, A.; Luntz, A. C.; Gowda, S. R.; Wallraff, G. M.; Garcia, J. M.; Mori, T.; Krupp, L. E. Combining Accurate O₂ and Li₂O₂ Assays to Separate Discharge and Charge Stability Limitations in Nonaqueous Li–O₂ Batteries. *J. Phys. Chem. Lett.* **2013**, *4*, 2989–2993.
- (28) Zhai, D. Y.; Wang, H.-H.; Yang, J. B.; Lau, K. C.; Li, K. X.; Amine, K.; Curtiss, L. A. Disproportionation in Li–O₂ Batteries Based on a Large Surface Area Carbon Cathode. *J. Am. Chem. Soc.* **2013**, *135*, 15364–15372.
- (29) Yilmaz, E.; Yogi, C.; Yamanaka, K.; Ohta, T.; Byon, H. R. Promoting Formation of Noncrystalline Li₂O₂ in the Li–O₂ Battery with RuO₂ Nanoparticles. *Nano Lett.* **2013**, *13*, 4679–4684.
- (30) Ding, Y.; Kim, Y. J.; Erlebacher, J. Nanoporous Gold Leaf: “Ancient Technology”/Advanced Materials. *Adv. Mater.* **2004**, *16*, 1897–1900.
- (31) Trahan, M. J.; Mukerjee, S.; Plichta, E. J.; Hendrickson, M. A.; Abraham, K. M. Studies of Li–Air Cells Utilizing Dimethyl Sulfoxide-Based Electrolyte. *J. Electrochem. Soc.* **2013**, *160*, A259–A267.
- (32) Black, R.; Lee, J. H.; Adams, B.; Mims, C. A.; Nazar, L. F. The Role of Catalysts and Peroxide Oxidation in Lithium–Oxygen Batteries. *Angew. Chem., Int. Ed.* **2012**, *52*, 392–396.

(33) Wang, R.; Yu, X. Q.; Bai, J. M.; Li, H.; Huang, X. J.; Chen, L. Q.; Yang, X. Q. Electrochemical Decomposition of Li_2CO_3 in $\text{NiO-Li}_2\text{CO}_3$ Nanocomposite Thin Film and Powder Electrodes. *J. Power Sources* **2012**, *218*, 113–118.